atmosphere

MDPI

Article

A Comprehensive Comparative Study on Evapotranspiration in Mainland Portugal Based on Climate Reanalysis Data

João Pedro Pegas [1,*], João Filipe Santos [2] and Maria Manuela Portela [3]

[1] Instituto Superior Técnico (IST), University of Lisbon, 1049-001 Lisbon, Portugal
[2] CREATE – Center for Sci-Tech Research in Earth System and Energy, Pole of the Polytechnic Institute of Beja, 7800-295 Beja, Portugal
[3] Instituto Superior Técnico (IST), Civil Engineering Research and Innovation for Sustainability (CERIS), 1049-001 Lisbon, Portugal
* Correspondence: joao.pegas@tecnico.ulisboa.pt

Abstract

Gridded meteorological data sources, such as reanalysis datasets, are increasingly used to estimate evapotranspiration, a key variable for surface water-budget analyses at regional and national scales and for assessing plant water requirements for irrigation. This study, conducted over mainland Portugal for the 44-year reference period from 1980 to 2023, first presents a comprehensive comparative analysis of the spatial patterns of potential (Ep) and reference (Eto) evapotranspiration at a 0.1° spatial resolution using daily data. Estimates derived from two high-resolution datasets (GLEAM and ERA5-Land) are compared with those obtained from the Thornthwaite, Hargreaves–Samani, and Penman–Monteith models. Secondly, trend analyses of Eto magnitudes on a monthly and annual basis in a grided format. The resulting spatial distributions of Ep and Eto show higher values in milder and flatter southern Portugal and lower values in the cooler and more mountainous northern regions, in agreement with existing knowledge. The Penman-Monteith model exhibited the highest reliability, while the Thornthwaite model generally underestimated evapotranspiration across the country and the Hargreaves-Samani model showed underestimation in coastal areas. Trend analysis of Eto indicates an overall increase in atmospheric evaporative demand over the full study period, with a more pronounced rise during the recent 22-year period (2002-2023) compared with the earlier period (1980-2001). These increases are statistically significant in August and October and may reflect a climate shift towards a progressively longer dry season. Understanding how changes in evapotranspiration affect hydrological processes - including surface water availability, river discharge, reservoir performance, and crop requirement - is critical. This study aims to contribute to addressing these emerging challenges.

Keywords: reference and potential evapotranspiration; gridded datasets; trend analysis; climate change

1. Introduction

Evapotranspiration is the process by which water is transferred from the earth to the atmosphere simultaneously through evaporation and plant transpiration involving both biological and physical mechanisms [1], which occur simultaneously, with the rates of both dependent on the atmosphere status, as well as the specific characteristics of soil,

crop and cultivation practices, and water availability. Different methods and models have been developed to estimate ~~the~~ evapotranspiration, each with its own advantages and applications, depending on the available data and goals [2–4], and involving more or fewer biophysical and atmospheric variables [5]. According to [6], the term potential evapotranspiration, Ep, refers to the maximum possible amount of ~~the~~ evapotranspiration considering the meteorological conditions, assuming complete vegetation cover and the absence of any limiting factors, such as soil moisture, nutrients, pest~~s~~, or disease~~s~~.

The most widely used agrometeorological variable in the fields of Hydrology, Agriculture and Climate science is the reference evapotranspiration, Eto [7], representing the evaporative demand of the atmosphere at a specific location and time of year, assuming a green reference surface and acting as a possible indicator of maximum potential evapotranspiration under ideal conditions in some climates [8]. With regard to its accuracy and the fact that it is widely recommended, the Food and Agriculture Organization of the United Nations (FAO) version of the Penman-Monteith Equation is the reference model for calculating Eto, since it is based on physical principles and includes physiological, radiation and aerodynamic components [9], and is also the basis for calculating crop evapotranspiration under standard and non-standard conditions.

The limited availability of meteorological records in many regions of the world has led to the development of models to calculate potential evapotranspiration, Ep, often aiming at approaching or comparing it with Eto, based on simpler equations, such as the empirical models of Thornthwaite [6] and Hargreaves-Samani [10], the latter was developed initially for a specific crop and location ~~as referred in~~ [9,10]. Although weather stations can provide accurate data at monitoring locations, spatial characterization analysis over large areas normally requires the application of interpolation methods. The availability of satellite climate data in recent years, has significantly advanced the ability to provide complete spatial, but also temporal, coverage, despite some recognized inaccuracy [11], especially in regions where in-situ measurements are sparse or non-existent. The Thornthwaite and Hargreaves-Samani models are widely applied because they use air temperature, which is a meteorological variable that is often available ~~based on relatively long time series of measurements~~.

Studies on the spatiotemporal characterization of evapotranspiration in various regions, including China, Pakistan, Ethiopia and the Iberian Peninsula, reveal significant trends and relevant climatic factors that affect Ep and Eto. In northern China, the spatiotemporal distribution characteristics and influencing factors of Eto in the Beijing–Tianjin–Hebei region from 1990 to 2019 was extensively studied by [12], to understand its implications on agricultural water management under climate change scenarios. The analysis revealed a significant downward trend in Eto, showing a decreasing trend of −3.07 mm/10 years, with Eto exhibiting a spatial distribution pattern that decreases from southwest to northeast. The study identifies temperature, wind speed, and sunshine hours as positively correlated with Eto, while relative humidity shows a negative correlation. Among these, wind speed and temperature are the dominant factors influencing Eto changes in the region. In Pakistan [13], the spatiotemporal characterization of Eto was assessed in Punjab, Pakistan, between 1950 and 2021, revealing significant variations influenced by climatic parameters. Eto was highest in southern Punjab, with minimum temperature being the dominant factor throughout the year, especially in winter. Similarly in Ethiopia, [14] presented a study on the spatiotemporal evaluation of two radiation-based and three temperature-based models for estimating potential evapotranspiration, Ep, against estimates of Eto by FAO Penman–Monteith model. Despite the high climatic variability in the Omo-Gibe basin case study, the results generally emphasized the superior performance of the simple temperature model, i.e., Hargreaves-Samani model, in capturing annual and seasonal Ep estimates. Annual Eto trends were also studied and

found to increase with the rising of temperature and the decreasing of relative humidity, wind speed, and solar radiation in some regions.

In the Iberian Peninsula, and particularly in mainland Portugal, where climate change has been accentuating irregularities in water availability and distribution, studies assessing the accuracy of new evapotranspiration products and the general characterization of the process involved play a crucial role in understanding the water cycle aiming at to improve water management efficiency, especially in agriculture, the main water consumer in the region [15]. As such, the work of [16] compared the Eto obtained with reanalysis data with the one derived based on data collected from 130 weather stations in the Iberian Peninsula. ~~The input climate variables obtained from the reanalysis were also compared with those observed for the same locations and ordinary kriging was used to estimate them in locations without observational data, due to a mismatched reanalysis data grid.~~ Also [17] studied the climatology and trends of the Eto over mainland Spain and the Balearic Islands, and the results showed low interannual variability, an accumulation of more than 50% of annual values in the summer, and a contribution of the radiative component to the Eto amount of more than 50%. A positive long-term trend over the period 1961-2014 has been detected for most of the study area but showing contrasting situations when shorter periods, of 20-30 years, were analysed. A seasonal analysis of the trends revealed also that spring and summer were the seasons showing long-term positive trends. The possible links between these pre-existing studies and the climate change effects in Portugal, using new datasets and longer time series, are necessarily important to deep seek.

Therefore, the objective ~~of this article is twofold.~~ ~~First~~, to develop a comparative analysis of the spatial patterns of the potential and reference evapotranspiration for ~~the first time in~~ mainland Portugal with a spatial resolution of 0.1° based on daily data and for a time span between 1980 and 2023. To this end evapotranspiration related-data from the GLEAM [18] and ERA5-Land reanalysis [19] datasets were analysed, together with estimates derived from the Thornthwaite and Hargreaves-Samani models, for Ep, and Penman-Monteith, for Eto [9], with the input variables obtained from ERA5-Land Copernicus Service catalogue. ~~Such results should support further analysis on the surface freshwater availability. In fact, previous studies [20] have shown that, when applying a water balance model, runoff estimates considering Eto or Ep separately were quite close, despite differences in evapotranspiration amounts.~~ The second objective is to perform a trend analysis of the magnitudes of Eto estimates, with the investigation emphasizing analysis on a monthly and annual basis in a grided format.

The results obtained allowed to evaluate the performance of the above-mentioned gridded products in estimating Ep and Eto, to compare different models and provide essential support and valuable information for scientific research in the fields of land-atmosphere interactions, hydrological modelling, and climate change studies at the national wide level.

2. Study Area

The comparative study on potential and reference evapotranspiration considered the continental territory of Portugal with approx. 89,015 km², as the study area. The country is located ~~in~~ the Iberian Peninsula, in the southwestern most part of Europe (between latitudes 36º and 42º N and longitudes 6º and 9º W), extending over a maximum length of about 561 km and an average width of 218 km (Figure 1a). Its borders are defined by Spain to the north and east, and by the Atlantic Ocean to the west and south. The coastline, oriented predominantly in a north–south direction, extends for more than 800 km.

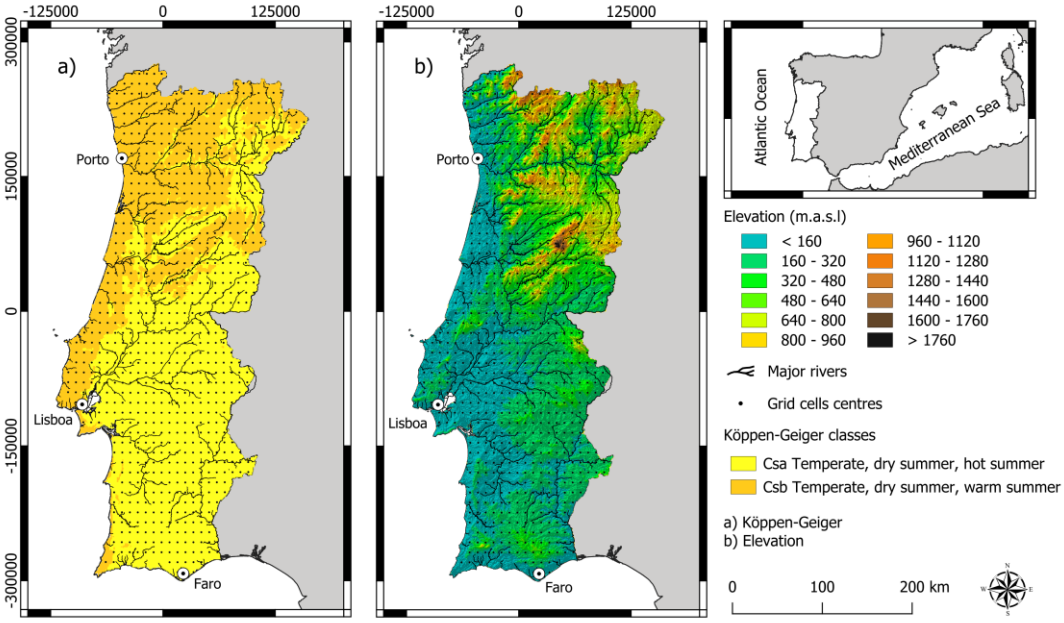

Figure 1. General location of Portugal with the black marks representing the 902 grid center points of the ERA5 Land dataset (0.1° resolution). a) Köppen-Geiger climate classification with 0.01º resolution, and b) Hypsometric map. Both illustrate the most important rivers and basins (coordinate referencing system: ETRS89 – TM06).

Despite the country's relatively small size, its geographical position allows for interaction between the climatic effects of the Atlantic and the Mediterranean [21]. There is a strong influence due to the proximity of the Atlantic Ocean and to the topography, with a central mountain range stretching from east to west, with elevations ranging from 0 to 2,000 meters above sea level. This mountain range divides a rugged northern region from a flatter southern region (Figure 1b). The prevailing Mediterranean climate is characterized by long, hot, dry summers and mild, relatively wet winters, characteristics that are more evident in the southernmost areas.

Rainfall is highly variable in both space and time, on seasonal and interannual scales. The mean annual rainfall is approximately 950 mm, but values range widely – from over 2,000 mm/year in some northwestern cooler regions to less than 500 mm/year in much of the warmer south, where water scarcity is a recurrent issue. Around 74% of the annual rainfall occurs during the wet ~~semester~~ (October–March), evenly distributed across its two quarters [22]. Maximum temperatures, reaching up to 45°C in summer, are observed in the southern inland regions, particularly along the border with Spain, while coastal and northern areas experience much more moderate temperatures. According to the Köppen–Geiger classification (for the period 1991–2020 [23]) the climate across most of mainland Portugal is classified as temperate (Csa and Csb classes) (Figure 1a).

3. Data Sources and Base Variables

The analysis of evapotranspiration (either Ep or Eto) magnitude and spatial pattern in mainland Portugal utilized data from GLEAM (version 4.1) and ERA5-Land reanalysis datasets. GLEAM has data on various components of evapotranspiration (www.gleam.eu), with the main objective of maximizing the retrieval of information associated with that variable available from satellite observations of different environmental and climatic variables [24]. The data retrieved from GLEAM was the potential evapotranspiration (Ep) covering the period from 1980 to 2023 with a spatial resolution of 0.1° × 0.1° (approximately 9 km × 9 km for ~~mainland~~ Portugal). ERA5-Land provides a view of the

evolution of the terrestrial water and energy cycles. It is produced by rerunning the land component of the ERA5 dataset [19] and combines model outputs with observations through a physics-based data assimilation process (reanalysis). The data, ~~including related to reference evapotranspiration~~ spans ~~from~~ from 1950 onwards, with the same spatial resolution as GLEAM. The shorter temporal coverage of the data provided by GLEAM compared to ERA5-Land constrained the definition of the study period ~~in mainland Portugal~~ from 1 January 1980 to 31 December 2023 (44 years), during which the two datasets overlap.

Regarding the reference evapotranspiration, [19] provides a link (https://data.bris.ac.uk/data/dataset/qb8ujazzda0s2aykkv0oq0ctp) to a repository developed by the University of Bristol, which offers global estimates of hourly and daily values derived using FAO's Penman–Monteith model applied to ERA5-Land meteorological data, covering a 44-year period, from 1981 to 2024. This period differs slightly from the study one, previously mentioned. Within the scope of this study, this product was also analysed and is referred to as Bristol.

The analysis of GLEAM and Bristol spatial datasets for mainland Portugal considered grid cells whose centroids were located within the country's borders, resulting in 902 overlaid cells. Both datasets were originally downloaded at a daily timescale. To ensure temporal consistency across years, February 29th of leap years was excluded from the time series.

Regardless of the time scale at which the data were retrieved or computed, and aiming to adopt a comparable and uniform temporal resolution, the maps of evapotranspiration, either Ep or Eto, derived from GLEAM, Bristol, or from the evapotranspiration models further described (section 4.1), were produced at a monthly scale, computed, when necessary, by aggregating daily values. Figure 2 presents the resulting evapotranspiration maps obtained from the first two aforementioned datasets (Ep from GLEAM and Eto from Bristol).

The spatially averaged monthly mean values obtained from the characterization presented in Figure 2 are 100.8 and 86.7 mm/month for GLEAM and Bristol, respectively. The corresponding mean annual evapotranspiration are 1209.6 mm/year and 1040.4 mm/year. The later estimate is comprehended in Eto characterization for mainland Portugal, which reported a spatial variation between 700 and 1200 mm/year [25].

The results used to produce the maps of Figure 2, were compared with those generated by applying three evapotranspiration estimation models, namely Thornthwaite [6], Hargreaves-Samani [10], and Penman-Monteith [9], further presented. The first two are empirical models mainly based on temperature, whereas the Penman-Monteith is a physically based model, as previously mentioned. For the implementation of these models, the required data were extracted from ERA5-Land. A daily time scale was adopted, with the exception of the data required by the Thornthwaite model which was retrieved from the ERA5-Land directly at the monthly time scale, compatible with the model requirements.

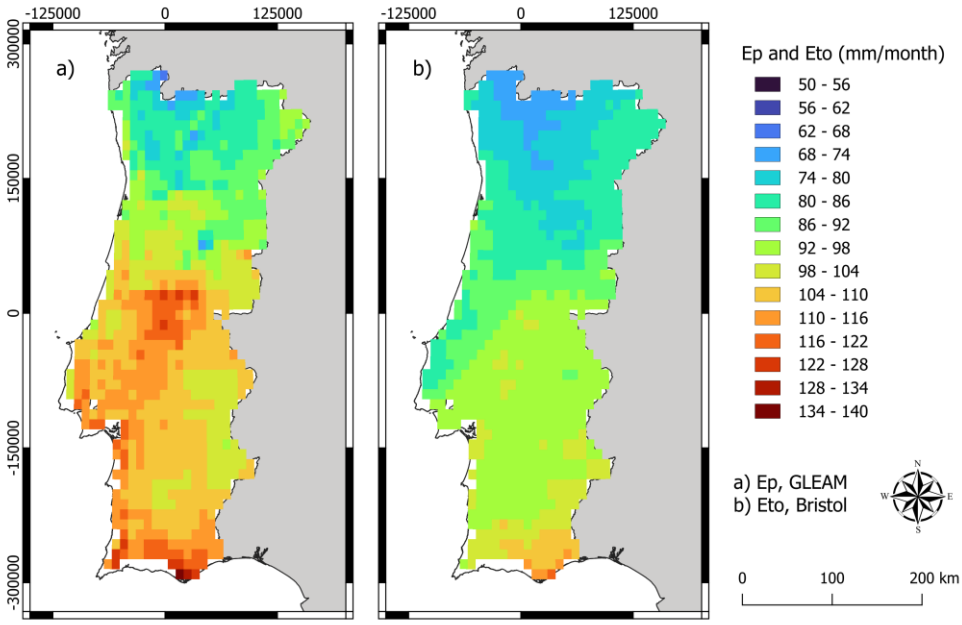

Figure 2. a) Ep from GLEAM (between 1st January 1980 to 31st December 2023) and b) Eto from Bristol (between 1st January to 1981 to 31st December 2024) mean monthly potential evapotranspiration maps (coordinate referencing system: ETRS89 – TM06).

The variables employed in the ~~aforementioned~~ models are identified in Table 1, together with the datasets from which they were extracted and the spatial and temporal resolution with which they were acquired, as well as the models that used these variables. The table also provides information on evapotranspiration, directly obtained from the Bristol and GLEAM datasets.

Table 1. Variables and datasets used to characterize the potential (Ep) and reference (Eto) evapotranspiration according to the models of Thornthwaite, Hargreaves-Samani, and Penman-Monteith.

Variable		Units	Data source (link to retrieve the data)	Spatial resolution	Time scale	Model
Symbol	Description					
Tm	2 meter average air temperature	°C	ERA5-Land (https://cds.climate.copernicus.eu/datasets/derived-era5-land-daily-statistics and https://cds.climate.copernicus.eu/datasets/reanalysis-era5-land-monthly-means)	0.1° x 0.1°	Month	Thornthwaite (Ep)
Tmin	2 meter minumum temperature	°C			Day	Hargreaves-Samani (Ep) and Penman-Monteith (Eto)
Tmax	2 meter maximum temperature	°C				
Tdew	2 meter dew point temperature	°C				Penman-Monteith (Eto)
P	Surface pressure	Pa				
Uu,10	10 meter wind velocity - U component	m/s				
Uv,10	10 meter wind velocity - V component	m/s				
Rns	Net solar radiation (short-wave)	J/m^2				
Rnl	Net thermal radiation (long-wave)	J/m^2				
Eto	Reference evapotranspiration	mm	Bristol (https://data.bris.ac.uk/data/dataset/qp8ujazda0s2aykkv0o0q0ctp)			
Ep	Pontential evapotranspiration	mm	GLEAM (https://www.gleam.eu/)			Penman (Ep)

Figure 3 provides the spatial characterization of the mean daily values of the variables listed in Table 1 over the 44-year period ~~from 1 January 1980 to 31 December 2023~~. The only exceptions are the minimum and maximum temperatures, which were replaced in each grid cell by their average (i.e., the mean daily temperature, further denoted as T).

The evapotranspiration directly given by Bristol and GLEAM reanalysis datasets were previously shown in Figure 2.

The analysis ~~of the maps of Figure 3~~ reveals a heterogeneous spatial pattern for all variables across mainland Portugal. The mean daily temperature, T, has its highest values in the southern inland regions and decreases toward the north and the coast. The mean daily dew point temperature, $Tdew$, is highest along the coastal areas and decreases toward the northeast. Surface pressure, P, displays a pronounced spatial gradient, with higher values along the coastal and southern inland regions, and lower values in the elevated northeastern areas following the expected topographic and coastal effects. $Uu, 10$, expresses the horizontal wind velocity component from west-east direction, heading east, assuming negative values when the wind blows opposite to the defined referential. The analysis indicates that, in terms of the mean daily values, west-to-east winds are more intense in the northwestern region of the country, while east-to-west winds are stronger in the coastal region south of Lisbon. $Uv, 10$ represents the vertical wind velocity component in the south-north direction, heading north, being negative whenever the wind blows opposite to the reference frame. It is observed that, across most of the country, the wind predominantly blows from north to south (the so-called "*Nortada*"), with higher intensities along the coastal areas. The net solar radiation (short-wave), Rns, takes positive values since it represents downward shortwave radiation emitted by the sun. It reaches higher intensities in the southern region and progressively decreases toward the north. According to ERA5-Land dataset, net thermal radiation (long-wave), Rnl, assumes negative values because the positive reference for radiation fluxes is defined downward, while this type of radiation is emitted upward from the Earth's surface. Rnl attains higher magnitudes in the southern inland region of the country and lower ones in the northern region. Finally, the radiation on top-of-atmosphere, Ra, depends only on latitude when considering mean daily values - see Equation (8) -, reaching higher magnitudes in the south and decreasing toward the northern regions.

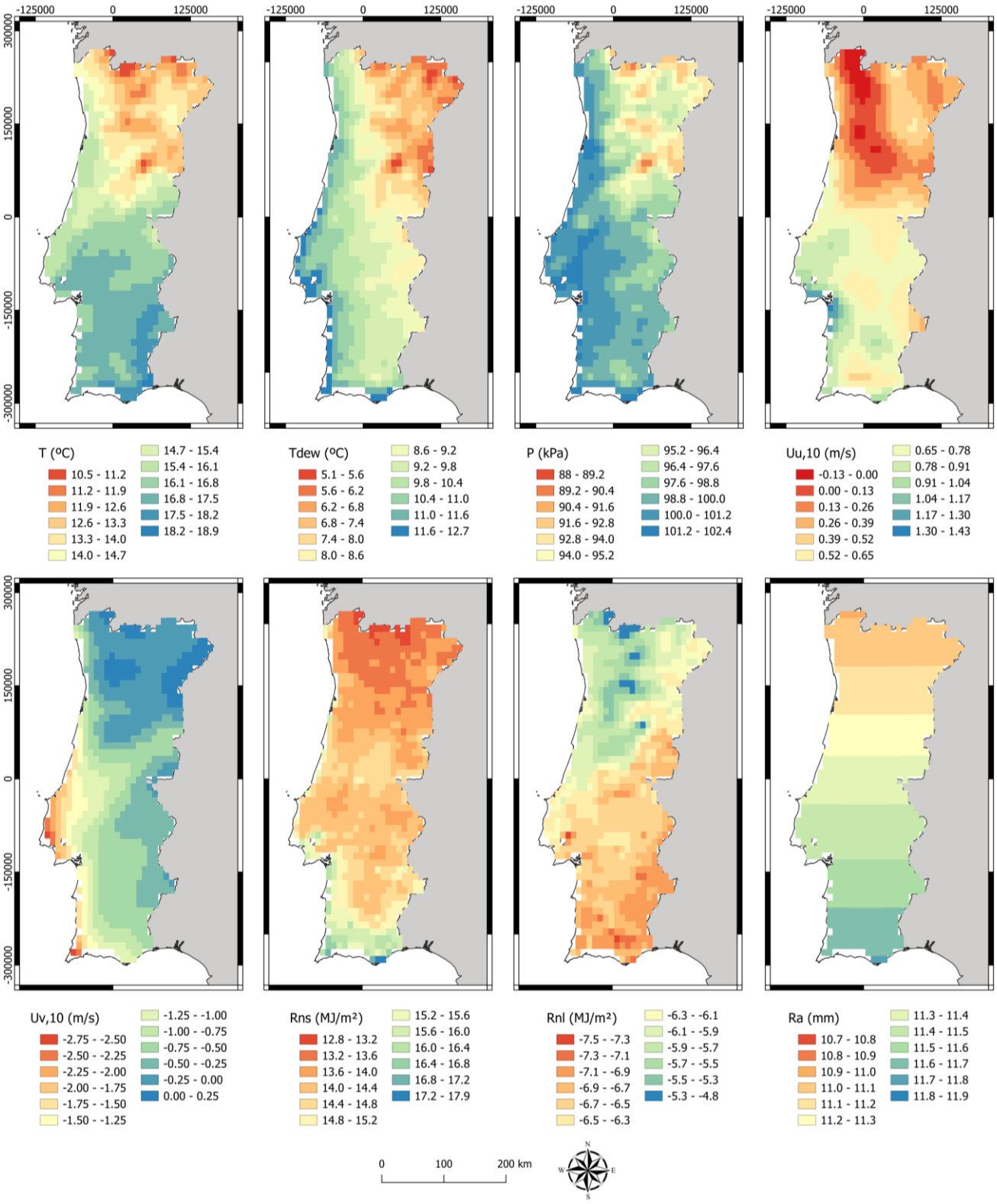

Figure 3. Maps of the mean daily values of the variables used to compute Ep and Eto over the 44-year period from 1 January 1980 to 31 December 2023. Symbols according to Table 1 (coordinate referencing system: ETRS89 – TM06).

4. Methods

4.1. Potential Evapotranspiration Models

The Thornthwaite model [6] was one of the first empirical models widely regarded as a simple method for estimating *Ep* [10,26]. Considering only the average monthly

temperature as a variable capable of expressing the energy balance, the model is especially recommended for an initial monthly estimate of Ep. At a location on the equator, a 30-day month, and an astronomical day length of 12 hours, Ep (mm) is expressed as:

$$Ep = 16\left(10\ \frac{Tm}{I}\right)^{a} \quad (1)$$

where:

Tm – mean monthly temperature (°C).

I – annual thermal index, given by the sum of the monthly thermal indices (i) calculated in each month based on the mean monthly temperature, according to:

$$i = \left(\frac{Tm}{5}\right)^{1.514} \quad (2)$$

This original equation is limited to the climatic conditions for which it was developed, and it leads to underestimates for arid conditions and overestimates for tropical and subtropical climate conditions [27]. To overcome this limitation the obtained values should be corrected by a factor that takes into account the month and the respective astronomical day length to be considered, according to:

$$f = \frac{Dm}{30}\ \frac{N}{12} \quad (3)$$

where:

Dm – number of days in the month considered (days);

N – astronomical day length (h).

To determine the astronomical day length, N, it is necessary to calculate the solar declination, δ, which depends on the Julian day under consideration. Such declination can be computed using the following equation [28]:

$$\delta = 23.45\ sin\left[\frac{360}{365}\ (J + 284)\right] \quad (4)$$

where:

δ – solar declination (°);

J – Julian day [number of the day in the year between 1 (1 January) and 365 (31 December).

In this study, the astronomical day length (N) was first computed in each month on a daily basis, and the corresponding monthly mean day length was then derived, in order to provide more accurate values than those typically obtained by considering only the 15th day of each month [6].

Based on the solar declination and the latitude for which the correction factor is to be determined, it is possible to calculate the sunset hour angle [9] by applying:

$$\omega = arcos\ (-tan\ (\varphi)\ tan\ (\delta)\ ) \quad (5)$$

where:

ω – sunset hour angle (°);

φ – latitude (°);

δ – solar declination (°).

The sunset hour angle represents the angle between the sun at the highest point of its trajectory and its position at sunrise or sunset. To convert this value into hours, it must be divided by 15 (15° corresponds to one hour). Taking this into account, the astronomical duration of the day can be obtained by [28]:

$$N = \frac{2\omega}{15} \quad (6)$$

where:

N – astronomical day length (h);

ω – sunset hour angle (°).

Once the astronomical duration of each day has been determined, it is possible to use Equation (3) to determine the dimensionless correction factor (f) to be applied to the Thornthwaite Ep given by Equation (1).

The Hargreaves-Samani model [10] is advantageous for estimating potential evapotranspiration in some climate types as it demonstrated superior performance compared to other models tested, making it particularly useful in regions where data availability is limited [29]. It has been also recommended whenever data required by Penman-Monteith Eto model are missing. The model can be expressed by:

$$\mathrm{Ep} = 0.0135\ \mathrm{Krs}\ \frac{\mathrm{Ra}}{\lambda}\ \sqrt{(\mathrm{Tmax} - \mathrm{Tmin})}\ (\mathrm{T} + 17.8) \quad (7)$$

In this study, the previous equation was applied at a daily time step, where T is the mean air temperature given by the average between the maximum ($Tmax$) and minimum ($Tmin$) air temperatures (°C); Ra is the top-of-atmosphere radiation at the latitude, day and location considered (MJ m^{-2} day^{-1}); λ is the latent heat of vaporization (2.5 MJ kg^{-1}); and Krs (°C$^{0.5}$) is the radiation coefficient, to which was assigned a value of 0.17, as proposed by [9,10] for semi-arid and subhumid climates. The constant 0.0135 converts US Customary (USC) to Metric (SI) units.

In order to estimate the top-of-atmosphere radiation (Ra) for each day of the year and for different latitudes, the solar constant and solar declination are also considered, according to the following equation [9]:

$$\mathrm{Ra} = \frac{24(60)}{\pi}\ \mathrm{Gsc}\ \mathrm{dr}\ [\omega \sin(\varphi) \sin(\delta) + \cos(\varphi) \cos(\delta) \sin(\omega)] \quad (8)$$

where:

Gsc – solar constant = 0.0820 MJ m^{-2} min^{-1};

dr – inverse relative distance Earth-Sun (au);

ω – sunset hour angle (°);

φ – latitude (°);

δ – solar declination (°).

The inverse relative distance Earth-Sun was computed based on [9]:

$$\mathrm{dr} = 1 + 0.033 \cos\left(\frac{2\pi}{365}\ \mathrm{J}\right) \quad (9)$$

The Penman-Monteith formulation for Eto at the adopted daily time step was the one described in [9] which follows FAO's Penman-Monteith Equation:

$$\mathrm{Eto} = \frac{0.408\ \Delta\ (\mathrm{Rn} - \mathrm{G}) + \gamma \frac{900}{\mathrm{T}+273}\ \mathrm{u}\ (\mathrm{es} - \mathrm{ea})}{\Delta + \gamma(1 + 0.34\ \mathrm{u})} \quad (10)$$

where:

Eto – reference evapotranspiration (mm day^{-1});

Rn – net radiation at the surface of the reference crop (MJ m^{-2} day^{-1});

G – heat flux density in ground (MJ m^{-2} day^{-1});

T – average air temperature at a height of 2 meter (°C);

u – wind speed at 2 meter height (ms^{-1}), given by the square root of Uu,10 and Uv,10;

es – vapor saturation pressure (kPa);

ea – current vapor pressure (kPa);

Δ – slope of the vapor pressure curve (kPa °C^{-1});

γ – psychometric constant (kPa °C^{-1}).

In the Penman-Monteith Eto calculation procedure the net radiation at the surface of the reference crop (Rn) was estimated from net solar (short-wave) radiation (Rns) and net thermal (long-wave) radiation (Rnl) according to:

$$\mathrm{Rn} = \mathrm{Rns} + \mathrm{Rnl} \quad (11)$$

Rnl assumes negative values, as explained in section 3. Since Rn expresses the balance between Rns and Rnl, it took negative values in approximately 11% of the grid cells, which in turn resulted in about 1% of negative daily Eto values that were replaced with zero. As the magnitude of the daily heat flux density in the ground (G) beneath the reference crop is relatively small, it may be ignored for 24-hour time steps [9]. For this reason, it was not included in the calculations ($G = 0$).

4.2. Trend Analysis

To assess the temporal stationarity of the Eto series, a trend analysis was conducted using the Mann–Kendall test [30,31] combined with the Sen's slope estimator [32,33]. The Mann–Kendall test is a rank-based non-parametric method used to detect the presence of monotonic trends in independent and randomly ordered time series. It does not depend on the data distribution, is robust to outliers, and, in its modified form, can accommodate autocorrelated series [34].

The magnitude of the trends, regardless of their statistical significance according to the Mann–Kendall test, was quantified using the Sen's slope estimator. This method computes the median of all possible pairwise slopes between data points, providing a robust and unbiased estimate of the rate of change over time.

The Mann–Kendall test was applied at each one of the 902 grid points to both monthly and annual Eto series. A significance level of 5% was adopted to identify statistically significant trends. Based on the Sen's slope results, a trend magnitude was assigned to each grid point and time scale and represented as maps, in which cells with significant trends are highlighted.

5. Results

5.1. Comparing Evapotranspiration Models

As mentioned earlier, the FAO version of the Eto Penman–Monteith model adopted in this analysis is considered to provide the most accurate estimate of the reference evapotranspiration. However, its implementation is highly demanding due to extensive data requirements, which constrain its applicability and highlight the need of simpler yet reliable models.

Within this context, a comparison was performed between mean monthly potential evapotranspiration estimated by each one of the two empirical approaches implemented (the Thornthwaite and Hargreaves–Samani models) and by the physically based Penman–Monteith reference evapotranspiration computed by using the variables of Table 1. The objective was to evaluate the performance of the empirical models in estimating atmospheric water demand. Such comparison allows for assessing the consistency between empirical and physically based estimates and provides guidance on alternative evapotranspiration models able ~~to be~~ applied in regions with limited meteorological data. The mean monthly Ep and Eto maps derived from the three models mentioned above are presented in Figure 4.

The spatially averaged monthly mean values obtained from the characterization presented in Figure 4 were 65.0, 87.4, and 85.8 mm/month for Thornthwaite, Hargreaves-Samani, and Penman-Monteith models, respectively. The corresponding mean annual evapotranspiration values were 780.0, 1048.0, and 1029.6 mm/year.

By considering both Figures 2 and 4, it can be concluded that the Ep estimates derived from GLEAM, presented in Figure 2 a), appear unsuitable for mainland Portugal, as their spatial variability does not align with previously established theoretical knowledge. Specifically, the GLEAM spatial pattern suggests that the very hot inland southern region exhibits significantly lower potential evapotranspiration values than the mild southern coastal area, in contrast to all other evapotranspiration characterizations and the process's physics. The analysis also shows that the Thornthwaite model underestimates Ep across mainland Portugal compared to the other models, as reported by several authors for semi-dry climates (e.g. [26,35–37]), while the Hargreaves-Samani model underestimates Ep near coastal areas.

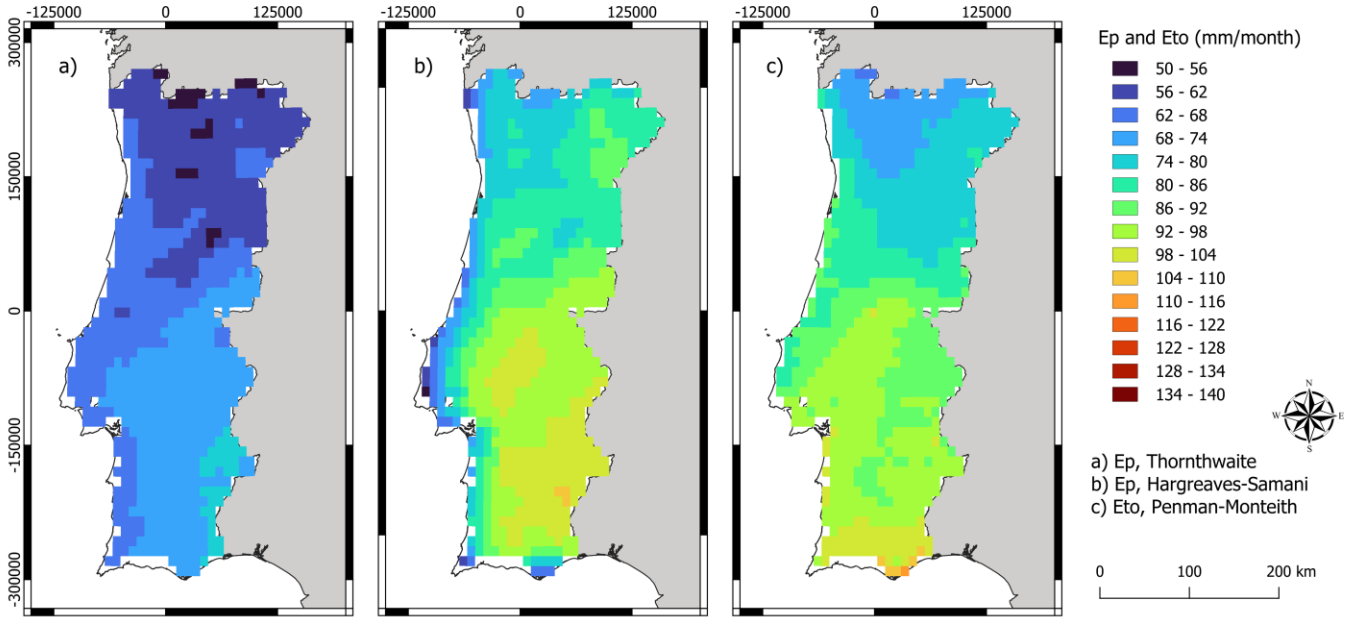

Figure 4. Mean monthly evapotranspiration maps (1st January to 1980 to 31st December 2023): Thornthwaite and Hargreaves-Samani (a and b) for Ep and Penman-Monteith model (c) for Eto (coordinate referencing system: ETRS89 – TM06).

The last discrepancy can be explained by the fact that the Hargreaves-Samani model relies on top-of-atmosphere radiation, which depends only on latitude, and on temperature, which is lower near the coast [38,39]. In contrast, models that account for wind velocity do not exhibit this coastal underestimation because wind speed is typically higher near the coast, an effect that is even more pronounced in Portugal due to the predominant west-east wind direction combined with a coast oriented almost entirely north-south, i.e. perpendicular to the wind direction.

To enable a more effective comparison between mean monthly evapotranspiration estimates, dimensionless differences were calculated ~~taking as reference~~ the computed Eto Penman–Monteith estimates, according to the following Equation:

$$\text{Diff} = \frac{(\text{Bristol or Ep}) - \text{Eto}}{\text{Eto}} \quad (12)$$

where:

$Diff$ – dimensionless differences (-);

Bristol – reference evapotranspiration from Bristol dataset (mm/month);

Ep – potential evapotranspiration derived from Thornthwaite or Hargreaves-Samani models (mm/month);

Eto – reference evapotranspiration estimates by the Penman-Monteith model (mm/month).

GLEAM Ep was not included in the analysis due to the inadequacy of its spatial pattern in mainland Portugal, as previously mentioned. The results from Equation (12) are presented as maps in Figure 5.

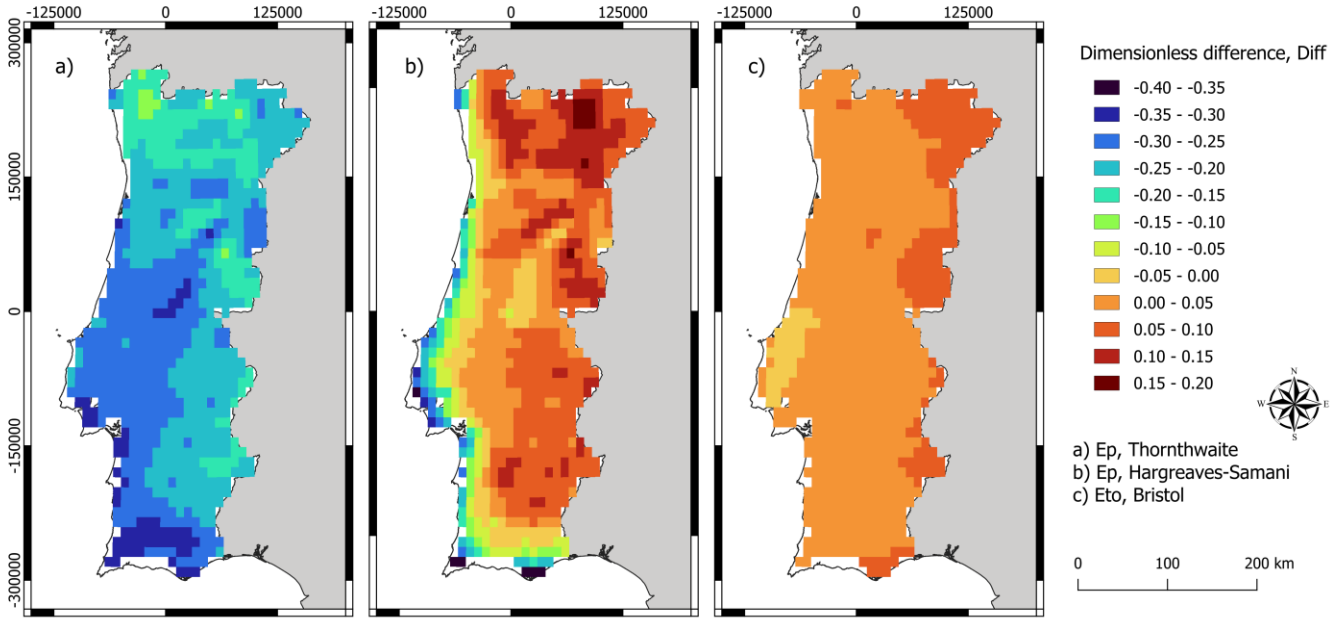

Figure 5. Differences between evapotranspiration estimates from Thornthwaite (a), Hargreaves-Samani (b) and Bristol (c) models, normalized with respect to the Penman–Monteith model estimates (coordinate referencing system: ETRS89 – TM06).

As shown in Figure 5, the Thornthwaite model for Ep presents normalized differences with respect to the Eto Penman-Monteith ranging from approximately -5% to -35% reinforcing the previously mentioned underestimation of the former model. These deviations are particularly pronounced under higher evapotranspiration demand constraints (south of Portugal), further highlighting the limitations of the Thornthwaite model. The more pronounced dimensionless differences of the Hargreaves-Samani model occur along the coast, suggesting poorer performance of the model in these windy areas, possibly due to the fact that it does not account for wind velocity in its formulation, as already mentioned. In contrast, the normalized differences for the Bristol dataset are small, only between -5% and +10%, supporting the suitability and reliability of this dataset for characterizing the reference evapotranspiration in mainland Portugal.

With the exception of a worse performance along the coastline and in very small northern and inland areas, the normalized differences of the Hargreaves-Samani model in the rest of the territory are less than 15% which indicates that, in the absence of the data required to compute Penman-Monteith Eto, the Hargreaves-Samani model can provide acceptable estimates of the reference evapotranspiration.

Given the relevance of the Penman-Monteith evapotranspiration model [9], an analysis was conducted to assess the relative sensitivity (RS) of the main input variables in the estimates of Eto, according with Equation (10), as previously study by [40] and [41]. For this purpose, Penman-Monteith evapotranspiration was recalculated at a monthly time scale. The assessment was performed by conducting a sensitivity analysis or "*one-at-a-time*" process at the monthly level, computed according with the following equation:

$$\mathrm{RS} = \left|\left(\frac{\mathrm{Eto}\,(\theta + \Delta\theta) - \mathrm{Eto}\,(\theta)}{\Delta\theta}\right)\left(\frac{\theta}{\mathrm{Eto}\,(\theta)}\right)\right| \quad (13)$$

where:

θ – monthly value of the variable without the increment;

$\Delta\theta$ – increment of the variable;

$Eto\,(\theta)$ – reference evapotranspiration estimates by the Penman-Monteith model without the increment in the variable (mm/month);

$Eto\ (\theta + \Delta\theta)$ – reference evapotranspiration estimates by the Penman-Monteith model with the increment in the variable (mm/month);

The analysis was computed for each month and grid cell and for the following input variables: net radiation at the surface of the reference crop (Rn), mean air temperature (T), and wind speed (u), both at 2 meter height. The mean results for the set of 902 grid cells are presented in Figure 6 in the form of a map of relative sensitivity (RS) for 1 % increment of the previously mentioned variables. For each variable, the spatial pattern for an increment of 5% is indistinguishable from the one of 1%, regardless of the variable under consideration.

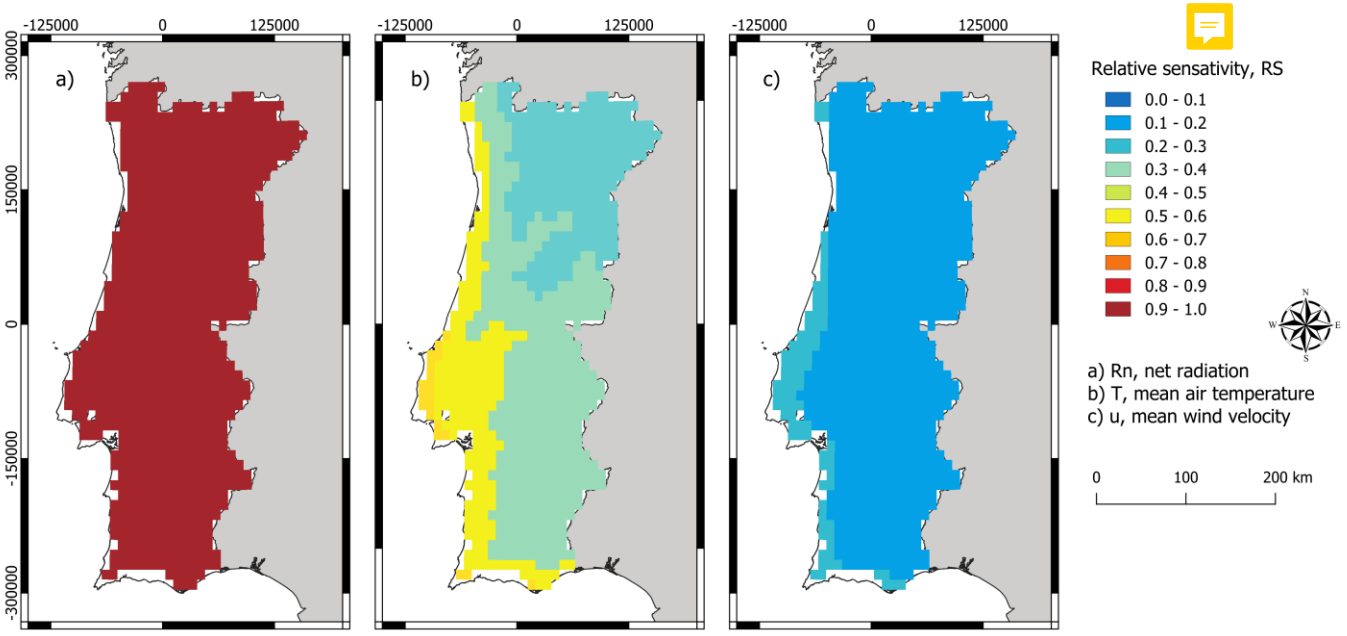

Figure 6. Mean monthly values of the relative sensitivity, RS, for 1% increment of some of the FAO's Penman-Monteith input variables: a) Rn, b) T, and c) u (coordinate referencing system: ETRS89 – TM06).

The spatially averaged relative sensitivity values obtained from the characterization presented in Figure 6 were 0.97, 0.45, and 0.15 for Rn, T, and u, respectively, and are nearly identical to those obtained considering an increment of 5%. These results indicate that net radiation has the strongest influence and therefore requires the most accurate measurement, followed by mean air temperature and wind velocity. However, it must be taken into account that Rn influences air temperature, and air temperature partly reflects radiation, so there is a one-way dependency. The wind speed u of the aerodynamic term of the Equation (10) presents very small relative sensitivity values.

The important relative contribution of the radiation term to Eto estimates was also assessed based on Equation (10). For the entire set of grid cells and daily estimates, it accounted for c.a. 60%, clearly stressing the role of Rn in the atmospheric water demand in mainland Portugal. This indicates that Eto is highly sensitive to Rn. A similar contribution of more than 50% of the radiation term to the annual Eto was obtained for mainland Spain as mentioned by [17].

5.2. Trend Analysis

As previously described, the Mann–Kendall test and Sen's slope estimator were used to assess trend magnitude and statistical significance. These analyses were applied to the monthly and annual Eto values derived from the Penman–Monteith model, for the 902

grid ~~cells. Figure 7 presents the results for the 44-year study period.~~ Trend magnitudes, regardless their significance, are indicated by the color scale. Significant trends (p-value<0.05) are highlighted by a black or white dot at the center of the corresponding cell, except ~~in case~~ when a note ~~explecitly~~ clarifies that all cells exhibit significant trends.

The mean monthly spatial averaged trends (mm/decade) sequentially from January to December are (Table 2): 0.12, 1.34, –0.12, 1.18, 6.49, 1.83, 3.72, 3.91, 0.22, 1.24, 0.38, and –0.14. For the annual series, the mean spatial averaged trend is 1.95 mm/year. Figure 7 shows that May exhibits the highest positive trends, with all grid cells displaying statistically significant values (p-value<0.05). In contrast, no statistically significant trends were identified for January, March, April, September, or December.

At the annual scale, the increase in Eto is unequivocal, with all trends statistically significant, indicating a robust and persistent rise in atmospheric evaporative demand over the past four decades, ~~in line with the results for Portugal from global [42] and regional [43] studies, within partial overlapped time windows and with remote or observational data.~~

To better interpret the observed evapotranspiration trends and detect possible temporal and spatial changes in the trends, the monthly and annual analysis was done considering two 22-year sequential sub-periods namely from 1980 to 2001 ~~(the former period)~~ and from 2002 to 2023 ~~(the more recent period)~~. ~~The results are presented in Figure 8 and 9, respectively.~~

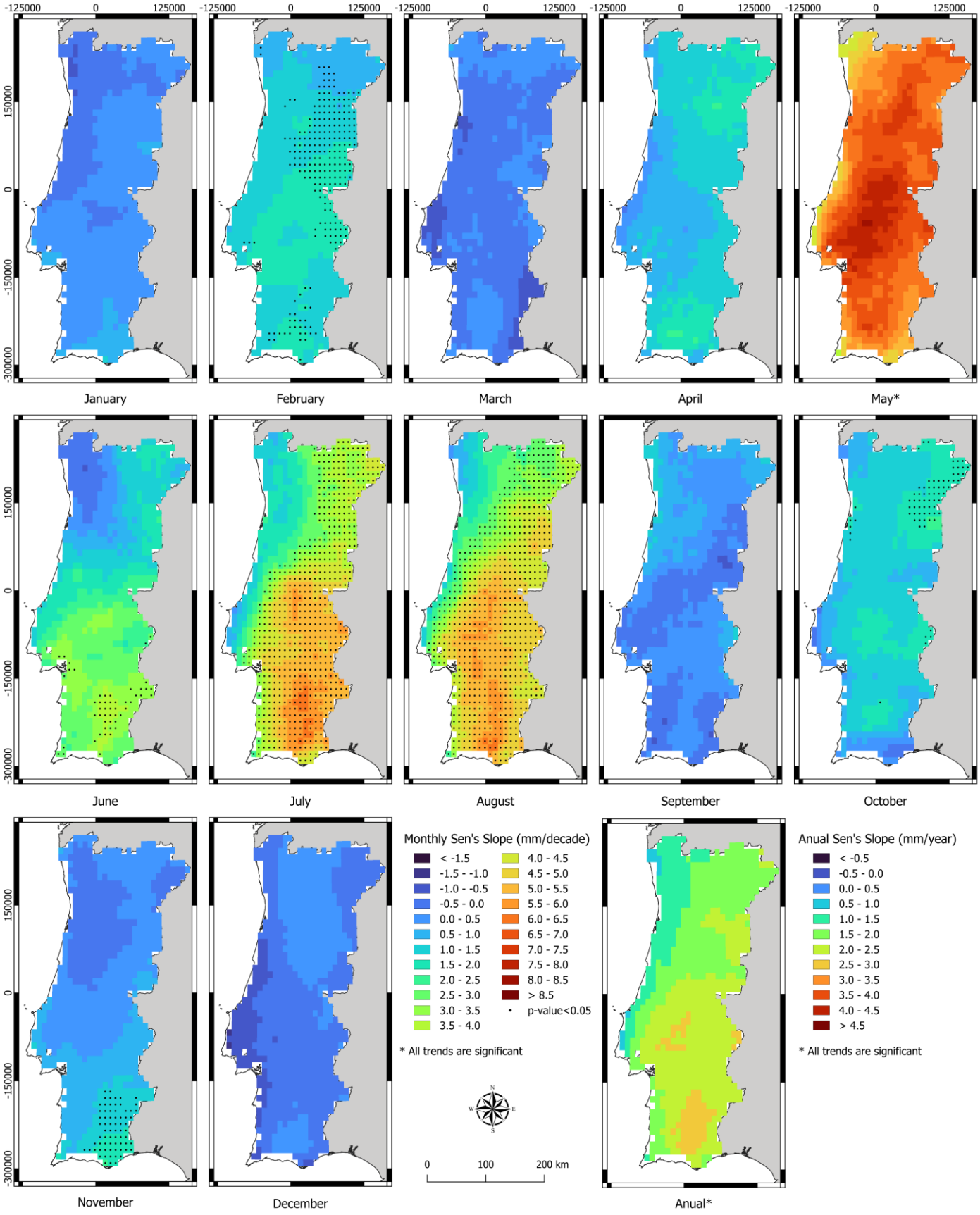

Figure 7. Trends in Eto Penman–Monteith reference evapotranspiration computed for each month and for the year over the study period (1980–2023). Grid cells with statistically significant trends are identified by a dot or by a note (coordinate referencing system: ETRS89 – TM06).

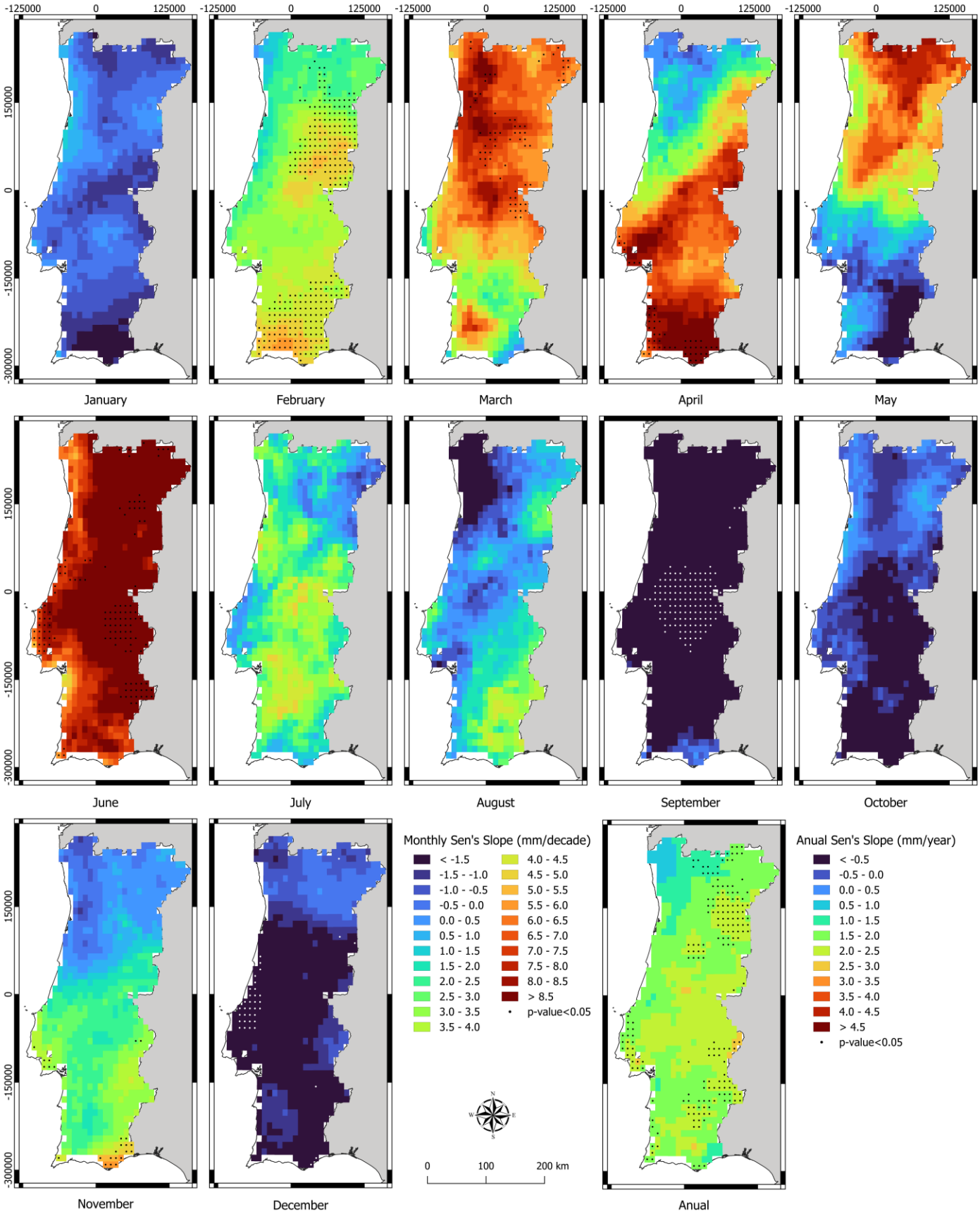

Figure 8. Trends in Eto Penman–Monteith reference evapotranspiration computed for each month and for the year over the former sub-period (1980–2001). Grid cells with statistically significant trends are identified by a dot or by a note (coordinate referencing system: ETRS89 – TM06).

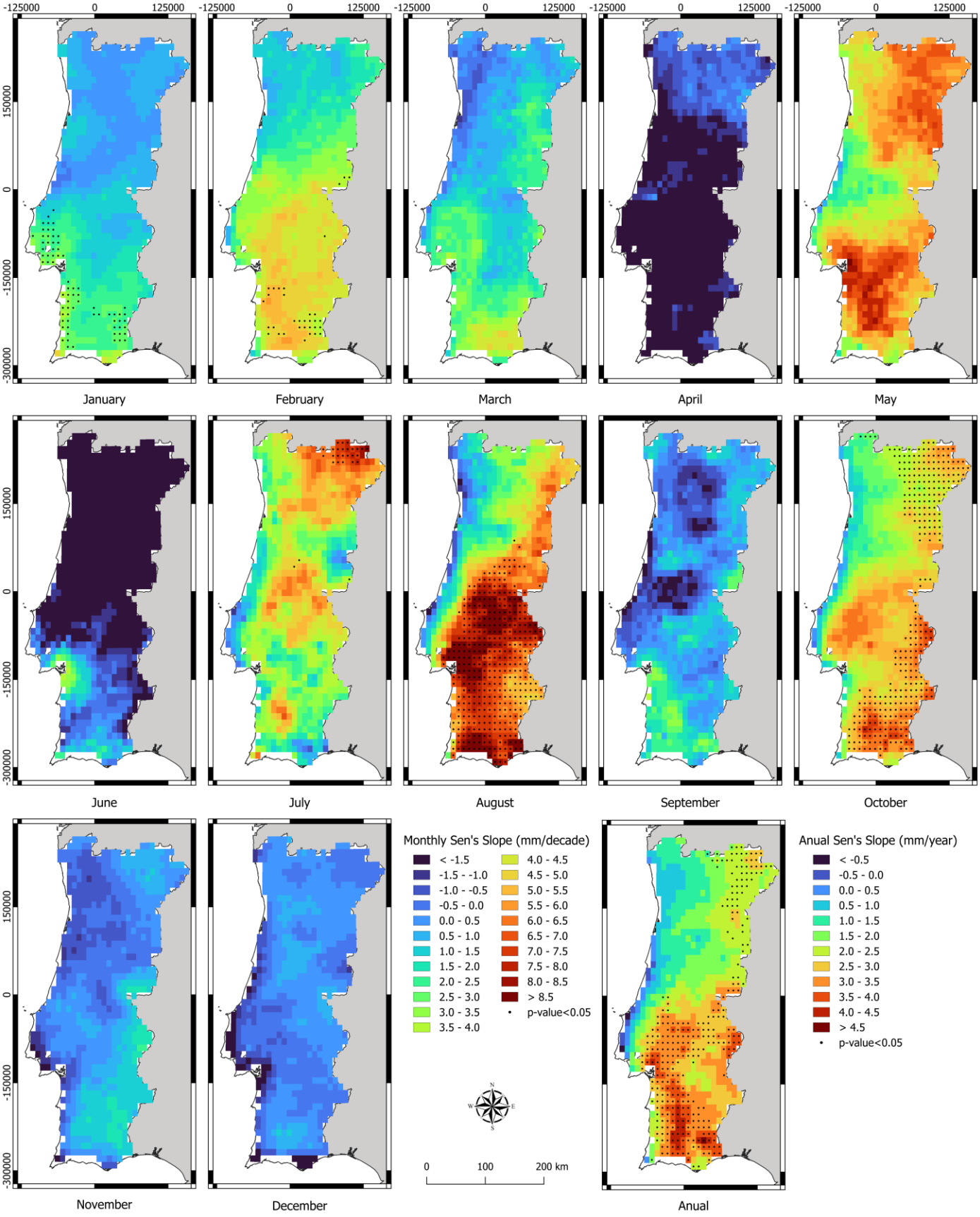

Figure 9. Trends in Eto Penman–Monteith reference evapotranspiration computed for each month and for the year over the more recent sub-period (2002–2023). Grid cells with statistically significant trends are identified by a dot or by a note (coordinate referencing system: ETRS89 – TM06).

https://doi.org/10.3390/xxxxx

For the study period and sub-periods – 1980 to 2023, 1980 to 2001, and 2002 to 2023 - Table 2 enables a comparison of Eto monthly and yearly trend magnitudes based on spatially averaged values, together with the percentage of grid cells exhibiting statistically significant trends.

Table 2. Summary of percentage of grid cells with Eto statistically significant trends and spatially averaged Eto trends for the analysed period and sub-periods (1980–2023, 1980–2001, and 2002–2023), for both the monthly and yearly scales.

	1980-2023		1980-2001		2002-2023	
	Significiant trends (%)	Mean trend (mm/decade)	Significiant trends (%)	Mean trend (mm/decade)	Significiant trends (%)	Mean trend (mm/decade)
January	0.00	0.12	0.00	-0.57	7.98	1.20
February	26.50	1.34	32.82	3.42	3.66	3.13
March	0.00	-0.12	7.43	5.76	0.00	1.54
April	0.00	1.18	5.54	5.03	0.00	-2.05
May	100.00	6.49	0.00	3.11	0.00	5.16
June	5.65	1.83	14.16	9.03	0.00	-3.14
July	71.62	3.72	0.00	2.23	2.99	3.77
August	83.48	3.91	0.00	0.69	44.60	5.16
September	0.00	0.22	14.41	-4.67	0.00	0.40
October	7.98	1.24	0.00	-1.31	35.92	4.34
November	7.76	0.38	2.66	1.62	0.00	0.21
December	0.00	-0.14	4.10	-1.57	0.00	-0.06
	Significiant trends (%)	Mean trend (mm/year)	Significiant trends (%)	Mean trend (mm/year)	Significiant trends (%)	Mean trend (mm/year)
Anual	100.00	1.95	21.40	1.87	35.03	2.24

The comparison between the sub-periods 1980 to 2001 and 2002 to 2023 highlights a clear intensification in Eto increasing trends in the most recent sub-period. In the former period, positive trends are more moderate and spatially variable, particularly during spring and early summer, with statistical significance occurring in more localized regions. In the more recent period, however, trends become stronger, spatially coherent, and widely significant, especially in July, August, and October. The months of August and October show clear evidence of increasing trends with statistical significance in inland areas, especially in the South. This pattern suggests a prolongation of summer-like conditions, possibly due to a stronger influence of heat events that result in greater demand for water by the atmosphere. Seasonal analysis confirms that the most substantial increase in Eto trend occurs during summer and beginning of autumn, whereas winter and spring maintain weak trends despite the sharp reversal in April, when the signal turned negative in the last period, perhaps due to an increase in relative humidity associated with higher precipitation.

~~These findings carry important implications for water resources and agricultural management. Higher Eto during critical growing months can intensify crop water stress, reduce soil moisture availability, and increase pressure on irrigation systems and reservoirs which become less reliable. The acceleration of trends after 2002 is consistent with the observed rise in the frequency of hot and dry years in Portugal reported by other authors [44–47] underscoring the need for adaptation in water planning and agricultural practices. Overall, the widespread and statistically significant increasing trends in Eto indicate that the atmospheric demand for water has become progressively stronger, particularly in the last two decades, potentially amplifying the impacts of climate change on water availability and agricultural productivity.~~

6. Discussion and Conclusions

For a precise evaluation of the hydrological processes involved in water and energy balance, the accuracy in the estimation of the reference and potential evapotranspiration, Eto or Ep, coupled with the choice of data sources to be used for that purpose are often points of uncertainty. This study conducted a comparative analysis of the performance of two global Eto and Ep products, Bristol, and GLEAM, along with estimates of common empirical models across mainland Portugal.

The results highlight the importance of selecting appropriate evapotranspiration data and contribute to a better understanding of the advantages and limitations of each product under specific environmental conditions, since these are a crucial biophysical process for assessing future changes in the water cycle.

Regardless of the dataset considered, the overall distribution of Eto or Ep in mainland Portugal shows higher values in the southern region and lower values in the northern region, in spatial agreement with previous studies for Portugal and ~~for~~ the Iberian Peninsula [16,48–50]. However, the diversity of models coupled with the short time scale and high spatial resolution of the datasets used in the present study offers a more in-depth view of the magnitude and spatial distribution of that important climatic variable over the country.

As mentioned, the Penman-Monteith model for estimating the reference evapotranspiration is widely regarded as a superior method due to its comprehensive formulation, which integrates multiple meteorological variables, therefore providing more accurate and reliable results, which is particularly relevant in regions with diverse climatic conditions. This also applies to Portugal [20,51]. For this reason, the study adopted Eto Penman-Monteith formulation as the reference for comparing the different evapotranspiration models. To this end, there are a variety of studies in the literature that precisely evaluate the performance of the Penman-Monteith in comparison with other models [52–55].

In general, the applied models reproduced the expected climatic and spatial gradients of evapotranspiration ~~in Portugal~~. However, differences in magnitude can be significant, as seen in the case of the Thornthwaite model for Ep, which relies solely on temperature, indicating that the inclusion of additional meteorological variables is important in explaining the process.

The clear exception ~~in model´s~~ performance was the GLEAM dataset which does not agree with the overall spatial gradient accepted for Portugal and obtained with all the aforementioned models, as it seems to overestimate Ep in coastal areas when compared to hotter inland, especially in the southern inland regions. This is in disagreement with other studies such as [56], that has validated the performance of the GLEAM product under extreme climatic conditions worldwide, or [57] that has ~~showed~~ the better performance of GLEAM 3.6 and of a Penman–Monteith derivative model on a yearly scale within five datasets based on ground and satellite observations for the USA. According to [18] there are key limitations that might impact the applicability of GLEAM model and its performance, such as the accuracy of satellite input data, especially in regions with limited availability of satellite and in situ observations.

Hargreaves' underestimation of Ep along the coastline or maritime-influenced conditions is an already known pattern in the bibliography, as the works of [58] for Andaluzia in southern Spain, [59], for Gangwondo province in South Korea, or [60], in coastal areas of Karachi, Gawadar, Jiwani and Pasni stations in Pakistan ~~as~~ already recognized. Nevertheless, the Hargreaves-Samani performance was in general the best among the two empirical models of Ep, clearly indicating that, in the absence of the data required to compute Penman-Monteith Eto, the Hargreaves-Samani model can provide acceptable estimates of the reference evapotranspiration [61,62].

Despite the recognition that the Thornthwaite method overestimates the potential evapotranspiration in humid climates, and underestimates it in arid climates [39,63,64]

some efforts have been made to adjust the parameters of the empirical formulation to better suit different climatic zones [27,65,66]. In the present study a more reliable calculation of the astronomical day length was conducted, by first computing it on a daily basis and then a corresponding monthly mean day length was derived, rather than the traditional calculation for the 15th day of each month [6]. The underestimation observed for Thornthwaite model may stem from its reliance solely on temperature data and its inability to account for aerodynamic effects, which can lead to inaccuracies in regions with heterogeneous climatic conditions [64], such as Portugal.

However, previous studies [20] have clearly shown that, when applying a water balance model to Portugal, the runoff estimates obtained using Ep from the Thornthwaite model and those obtained using Eto from the Penman-Monteith model were very similar. This occurred despite substantial differences in evapotranspiration rates, because the water balance in Portugal is often limited mainly by the availability of surface water (i.e., precipitation) and not by the evapotranspiration process itself. Further studies based on the currently available and detailed datasets should address these early findings, for example by aiming to develop simpler models that can be applied to preliminary evaluate surface water availability or for the early-stage design of irrigation systems.

For trend analysis, the results for Portugal are in line with current analyses and observations suggesting a general increase in atmospheric evaporative demand on a global scale [42] and ~~in~~ the Iberian Peninsula [43,67]. This increase contributes to water scarcity and drought intensification, ultimately leading to an imbalance in the water budget [68]. The marked increase in the evapotranspiration upwards trend in recent years, compared to earlier years, is spatial widespread and particularly significant in August and October. This pattern portraits a changing climate that points toward a progressively longer dry season.

Knowing that the availability of surface freshwater will be significantly influenced by global warming [69,70], understanding how evapotranspiration trends may alter the hydrological processes and lead to important changes in streamflow and reservoir storage are pressing questions that needs to be answered.

Additionally, the impacts of climate variability on vegetation evapotranspiration, as well as the adaptability of different crops in irrigated areas, are also critical issues that require further investigation ~~in Portugal~~. A deeper understanding of these processes is essential for identifying crops better adapted and more resilient to climatic conditions, improving water-resources management, anticipating future agricultural demands, and supporting the development of resilient strategies and planning to face climate change.

Acknowledgments: This research was funded in whole or in part by the Fundação para a Ciência e a Tecnologia, I.P. (FCT, https://ror.org/00snfqn58) under Grant UID/6438/2025 of the research unit CERIS, and by the CERMA Erasmus+ Project N°. 2024-1-SK01-KA220-HED- 000243758 from the European Union.

References

1. Yang, F.; Zhang, Q.; Hunt, J.E.; Zhou, J.; Sha, S.; Li, Y.; Yang, Z.; Qi, Y.; Wang, X. Biophysical Regulation of Evapotranspiration in Semiarid Croplands. Journal of Soil and Water Conservation **2019**, 74, 309–318, doi:10.2489/jswc.74.3.309.
2. Pereira, L.S.; Perrier, A.; Allen, R.G.; Alves, I. Evapotranspiration: Concepts and Future Trends. J. Irrig. Drain Eng. **1999**, 125, 45–51, doi:10.1061/(asce)0733-9437(1999)125:2(45).
3. Wang, K.; Dickinson, R.E. A Review of Global Terrestrial Evapotranspiration: Observation, Modeling, Climatology, and Climatic Variability. Reviews of Geophysics **2012**, 50, doi:10.1029/2011rg000373.
4. Liou, Y.-A.; Kar, S. Evapotranspiration Estimation with Remote Sensing and Various Surface Energy Balance Algorithms—A Review. Energies **2014**, 7, 2821–2849, doi:10.3390/en7052821.
5. World Meteorological Organization State of Global Water Resources 2022; United Nations, 2023; ISBN 978-92-63-11333-7.

6. Thornthwaite, C.W. An Approach toward a Rational Classification of Climate. Geographical Review **1948**, 38, 55, doi:10.2307/210739.
7. Yao, M.-H.; Li, M.-H.; Juan, J.-Y.; Hsia, Y.-J.; Lee, P.-H.; Shen, Y. Mapping Reference Evapotranspiration from Meteorological Satellite Data and Applications. Terr. Atmos. Ocean. Sci. **2017**, 28, 501–515, doi:10.3319/TAO.2016.11.15.01.
8. Irmak, S.; Gabriela Arellano, M. Reference (Potential) Evapotranspiration. II: Frequency Distribution in Humid, Subhumid, Arid, Semiarid, and Mediterranean-Type Climates. J. Irrig. Drain Eng. **2016**, 142, 04015066, doi:10.1061/(ASCE)IR.1943-4774.0000979.
9. Allen, R.G.; Pereira, L.S.; Raes, D.; Smith, M. Crop Evapotranspiration: Guidelines for Computing Crop Water Requirements; Food and Agriculture Organization of the United Nations, Ed.; FAO irrigation and drainage paper; Food and Agriculture Organization of the United Nations: Rome, **1998**; ISBN 978-92-5-104219-9.
10. George H. Hargreaves; Zohrab A. Samani Reference Crop Evapotranspiration from Temperature. Applied Engineering in Agriculture **1985**, 1, 96–99, doi:10.13031/2013.26773.
11. Mendelsohn, R.; Kurukulasuriya, P.; Basist, A.; Kogan, F.; Williams, C. Climate Analysis with Satellite versus Weather Station Data. Climatic Change **2007**, 81, 71–83, doi:10.1007/s10584-006-9139-x.
12. Liu, Z.; Jing, D.; Han, Y.; Yu, J.; Lu, T.; Zhangzhong, L. Spatiotemporal Distribution Characteristics and Influencing Factors Analysis of Reference Evapotranspiration in Beijing–Tianjin–Hebei Region from 1990 to 2019 under Climate Change. Sustainability **2022**, 14, 6277, doi:10.3390/su14106277.
13. Ashraf, H.; Qamar, S.; Riaz, N.; Shamshiri, R.R.; Sultan, M.; Khalid, B.; Ibrahim, S.M.; Imran, M.; Khan, M.U. Spatiotemporal Estimation of Reference Evapotranspiration for Agricultural Applications in Punjab, Pakistan. Agriculture **2023**, 13, 1388, doi:10.3390/agriculture13071388.
14. Woldesenbet, T.A.; Elagib, N.A. Spatial-temporal Evaluation of Different Reference Evapotranspiration Methods Based on the Climate Forecast System Reanalysis Data. Hydrological Processes **2021**, 35, doi:10.1002/hyp.14239.
15. Fonseca, A.; Andrade, C.; Santos, J.A. Agricultural Water Security under Climate Change in the Iberian Peninsula. Water **2022**, 14, 768, doi:10.3390/w14050768.
16. Martins, D.S.; Paredes, P.; Raziei, T.; Pires, C.; Cadima, J.; Pereira, L.S. Assessing Reference Evapotranspiration Estimation from Reanalysis Weather Products. An Application to the Iberian Peninsula. Intl Journal of Climatology **2017**, 37, 2378–2397, doi:10.1002/joc.4852.
17. Tomas-Burguera, M.; Beguería, S.; Vicente-Serrano, S.M. Climatology and Trends of Reference Evapotranspiration in Spain. Intl Journal of Climatology **2021**, 41, doi:10.1002/joc.6817.
18. Miralles, D.G.; Holmes, T.R.H.; De Jeu, R.A.M.; Gash, J.H.; Meesters, A.G.C.A.; Dolman, A.J. Global Land-Surface Evaporation Estimated from Satellite-Based Observations. Hydrol. Earth Syst. Sci. **2011**, 15, 453–469, doi:10.5194/hess-15-453-2011.
19. Muñoz-Sabater, J.; Dutra, E.; Agustí-Panareda, A.; Albergel, C.; Arduini, G.; Balsamo, G.; Boussetta, S.; Choulga, M.; Harrigan, S.; Hersbach, H.; et al. ERA5-Land: A State-of-the-Art Global Reanalysis Dataset for Land Applications. Earth Syst. Sci. Data **2021**, 13, 4349–4383, doi:10.5194/essd-13-4349-2021.
20. Manuela Portela, M.; Santos, J.; Marinho De Carvalho Studart, T. Effect of the Evapotranspiration of Thornthwaite and of Penman-Monteith in the Estimation of Monthly Streamflows Based on a Monthly Water Balance Model. In Current Practice in Fluvial Geomorphology - Dynamics and Diversity; Gopal Ghosh, K., Mukhopadhyay, S., Eds.; IntechOpen, **2020** ISBN 978-1-78984-578-5.
21. Mora, C.; Vieira, G. The Climate of Portugal. In Landscapes and Landforms of Portugal; Vieira, G., Zêzere, J.L., Mora, C., Eds.; World Geomorphological Landscapes; Springer International Publishing: Cham, **2020**; pp. 33–46 ISBN 978-3-319-03640-3.
22. Portela, M.M.; Espinosa, L.A.; Zelenakova, M. Long-Term Rainfall Trends and Their Variability in Mainland Portugal in the Last 106 Years. Climate **2020**, 8, 146, doi:10.3390/cli8120146.
23. Beck, H.E.; McVicar, T.R.; Vergopolan, N.; Berg, A.; Lutsko, N.J.; Dufour, A.; Zeng, Z.; Jiang, X.; Van Dijk, A.I.J.M.; Miralles, D.G. High-Resolution (1 Km) Köppen-Geiger Maps for 1901–2099 Based on Constrained CMIP6 Projections. Sci Data **2023**, 10, 724, doi:10.1038/s41597-023-02549-6.
24. Miralles, D.G.; Bonte, O.; Koppa, A.; Baez-Villanueva, O.M.; Tronquo, E.; Zhong, F.; Beck, H.E.; Hulsman, P.; Dorigo, W.; Verhoest, N.E.C.; et al. GLEAM4: Global Land Evaporation and Soil Moisture Dataset at 0.1° Resolution from 1980 to near Present. Sci Data **2025**, 12, 416, doi:10.1038/s41597-025-04610-y.
25. Instituto Nacional da Água, I. Plano Nacional Da Água: Portugal Continental; Ministério Do Ambiente e Do Ordenamento Do Território: Lisboa, **2000**;

26. Almorox, J.; Quej, V.H.; Martí, P. Global Performance Ranking of Temperature-Based Approaches for Evapotranspiration Estimation Considering Köppen Climate Classes. Journal of Hydrology **2015**, 528, 514–522, doi:10.1016/j.jhydrol.2015.06.057.
27. Trajkovic, S.; Gocic, M.; Pongracz, R.; Bartholy, J. Adjustment of Thornthwaite Equation for Estimating Evapotranspiration in Vojvodina. Theor Appl Climatol **2019**, 138, 1231–1240, doi:10.1007/s00704-019-02873-1.
28. Forsythe, W.C.; Rykiel, E.J.; Stahl, R.S.; Wu, H.; Schoolfield, R.M. A Model Comparison for Daylength as a Function of Latitude and Day of Year. Ecological Modelling **1995**, 80, 87–95, doi:10.1016/0304-3800(94)00034-F.
29. Gurski, B.C.; Jerszurki, D.; Souza, J.L.M.D. Alternative Reference Evapotranspiration Methods for the Main Climate Types of the State of Paraná, Brazil. Revista Brasileira de Meteorologia **2018**, v. 33, n. 3, 567-578, doi: 10.1590/S0100-204X2018000900003.
30. Mann, H.B. Nonparametric Tests Against Trend. Econometrica **1945**, 13, 245, doi:10.2307/1907187.
31. Kendall, M.G. Rank Correlation Methods; 4. ed., 2. impr.; Griffin: London, **1975**; ISBN 978-0-85264-199-6.
32. Sen, P.K. Estimates of the Regression Coefficient Based on Kendall's Tau. Journal of the American Statistical Association **1968**, 63, 1379–1389, doi:10.1080/01621459.1968.10480934.
33. Raj, B.; Koerts, J. Henri Theil's Contributions to Economics and Econometrics: Econometric Theory and Methodology; Advanced Studies in Theoretical and Applied Econometrics; Springer-Science+Business Media: Dordrecht, **1992**; ISBN 978-94-010-5124-8.
34. Hamed, K.H.; Ramachandra Rao, A. A Modified Mann-Kendall Trend Test for Autocorrelated Data. Journal of Hydrology **1998**, 204, 182–196, doi:10.1016/S0022-1694(97)00125-X.
35. Pereira, A.R.; Pruitt, W.O. Adaptation of the Thornthwaite Scheme for Estimating Daily Reference Evapotranspiration. Agricultural Water Management **2004**, 66, 251–257, doi:10.1016/j.agwat.2003.11.003.
36. Valipour, M.; Gholami Sefidkouhi, M.A.; Raeini−Sarjaz, M. Selecting the Best Model to Estimate Potential Evapotranspiration with Respect to Climate Change and Magnitudes of Extreme Events. Agricultural Water Management **2017**, 180, 50–60, doi:10.1016/j.agwat.2016.08.025.
37. Aschonitis, V.; Touloumidis, D.; Ten Veldhuis, M.-C.; Coenders-Gerrits, M. Correcting Thornthwaite Potential Evapotranspiration Using a Global Grid of Local Coefficients to Support Temperature-Based Estimations of Reference Evapotranspiration and Aridity Indices. Earth Syst. Sci. Data **2022**, 14, 163–177, doi:10.5194/essd-14-163-2022.
38. Gavilán, P.; Lorite, I.J.; Tornero, S.; Berengena, J. Regional Calibration of Hargreaves Equation for Estimating Reference ET in a Semiarid Environment. Agricultural Water Management **2006**, 81, 257–281, doi:10.1016/j.agwat.2005.05.001.
39. Shiri, J.; Sadraddini, A.A.; Nazemi, A.H.; Marti, P.; Fakheri Fard, A.; Kisi, O.; Landeras, G. Independent Testing for Assessing the Calibration of the Hargreaves–Samani Equation: New Heuristic Alternatives for Iran. Computers and Electronics in Agriculture **2015**, 117, 70–80, doi:10.1016/j.compag.2015.07.010.
40. Irizarry-Ortiz, M.; Harmsen, E.W. Sensitivity of the Penman–Monteith Reference Evapotranspiration Equation to Meteorological Variables for Puerto Rico. Hydrology **2023**, 10, 101, doi:10.3390/hydrology10050101.
41. Rim, C.-S. Sensitivity Analysis of the FAO Penman-Monteith Reference Evapotranspiration Model. Journal of Korea Water Resources Association **2023**, 56, 285–299, doi:10.3741/JKWRA.2023.56.4.285.
42. Ma, N.; Szilágyi, J.; Zhang, Y. Hydrological Responses to Warming: Insights From Centennial-Scale Terrestrial Evapotranspiration Estimates. Water Resources Research **2025**, 61(9), doi:10.1029/2025wr041001.
43. Vicente-Serrano, S.M.; Lopez-Moreno, J.-I.; Beguería, S.; Lorenzo-Lacruz, J.; Sanchez-Lorenzo, A.; García-Ruiz, J.M.; Azorin-Molina, C.; Morán-Tejeda, E.; Revuelto, J.; Trigo, R.; et al. Evidence of Increasing Drought Severity Caused by Temperature Rise in Southern Europe. Environ. Res. Lett. **2014**, 9, 044001, doi:10.1088/1748-9326/9/4/044001.
44. Espírito Santo, F.; De Lima, M.I.P.; Ramos, A.M.; Trigo, R.M. Trends in Seasonal Surface Air Temperature in Mainland Portugal, since 1941. Intl Journal of Climatology **2014**, 34, 1814–1837, doi:10.1002/joc.3803.
45. Espinosa, L.A.; Portela, M.M.; Moreira Freitas, L.M.; Gharbia, S. Addressing the Spatiotemporal Patterns of Heatwaves in Portugal with a Validated ERA5-Land Dataset (1980–2021). Water **2023**, 15, 3102, doi:10.3390/w15173102.
46. Espinosa, L.A.; Portela, M.M. Red-Hot Portugal: Mapping the Increasing Severity of Exceptional Maximum Temperature Events (1980–2024). Atmosphere **2025**, 16, 514, doi:10.3390/atmos16050514.
47. Ramos, A.; Trigo, R.; Santo, F. Evolution of Extreme Temperatures over Portugal: Recent Changes and Future Scenarios. Clim. Res. **2011**, 48, 177–192, doi:10.3354/cr00934.
48. Espadafor, M.; Lorite, I.J.; Gavilán, P.; Berengena, J. An Analysis of the Tendency of Reference Evapotranspiration Estimates and Other Climate Variables during the Last 45 Years in Southern Spain. Agricultural Water Management **2011**, 98, 1045–1061, doi:10.1016/j.agwat.2011.01.015.

49. Vicente-Serrano, S.M.; Azorin-Molina, C.; Sanchez-Lorenzo, A.; Revuelto, J.; López-Moreno, J.I.; González-Hidalgo, J.C.; Moran-Tejeda, E.; Espejo, F. Reference Evapotranspiration Variability and Trends in Spain, 1961–2011. Global and Planetary Change **2014**, 121, 26–40, doi:10.1016/j.gloplacha.2014.06.005.
50. Azorin-Molina, C.; Vicente-Serrano, S.M.; Sanchez-Lorenzo, A.; McVicar, T.R.; Morán-Tejeda, E.; Revuelto, J.; El Kenawy, A.; Martín-Hernández, N.; Tomas-Burguera, M. Atmospheric Evaporative Demand Observations, Estimates and Driving Factors in Spain (1961–2011). Journal of Hydrology **2015**, 523, 262–277, doi:10.1016/j.jhydrol.2015.01.046.
51. Andrade, J.A.; Ventura, R. Estimation Of Reference Evapotranspiration By Hargreaves-Samani And Penman-Monteith Methods In Mediterranean Environment (Portugal). Finisterra **2024**, E33850 Páginas, doi:10.18055/Finis33850.
52. Giménez, P.O.; García-Galiano, S.G. Assessing Regional Climate Models (RCMs) Ensemble-Driven Reference Evapotranspiration over Spain. Water **2018**, 10, 1181, doi:10.3390/w10091181.
53. Djaman, K.; Balde, A.B.; Sow, A.; Muller, B.; Irmak, S.; N'Diaye, M.K.; Manneh, B.; Moukoumbi, Y.D.; Futakuchi, K.; Saito, K. Evaluation of Sixteen Reference Evapotranspiration Methods under Sahelian Conditions in the Senegal River Valley. Journal of Hydrology: Regional Studies **2015**, 3, 139–159, doi:10.1016/j.ejrh.2015.02.002.
54. Samaras, D.A.; Reif, A.; Theodoropoulos, K. Evaluation of Radiation-Based Reference Evapotranspiration Models Under Different Mediterranean Climates in Central Greece. Water Resour Manage **2014**, 28, 207–225, doi:10.1007/s11269-013-0480-3.
55. Maestre-Valero, J.F.; Martínez-Alvarez, V.; González-Real, M.M. Regionalization of the Hargreaves Coefficient to Estimate Long-Term Reference Evapotranspiration Series in SE Spain. Span. j. agric. res. **2013**, 11, 1137–1152, doi:10.5424/sjar/2013114-3869.
56. Qian, L.; Zhang, Z.; Wu, L.; Fan, S.; Yu, X.; Liu, X.; Ba, Y.; Ma, H.; Wang, Y. High Uncertainty of Evapotranspiration Products under Extreme Climatic Conditions. Journal of Hydrology **2023**, 626, 130332, doi:10.1016/j.jhydrol.2023.130332.
57. Chao, L.; Zhang, K.; Wang, J.; Feng, J.; Zhang, M. A Comprehensive Evaluation of Five Evapotranspiration Datasets Based on Ground and GRACE Satellite Observations: Implications for Improvement of Evapotranspiration Retrieval Algorithm. Remote Sensing **2021**, 13, 2414, doi:10.3390/rs13122414.
58. Aguilar, C.; Polo, M.J. Generating Reference Evapotranspiration Surfaces from the Hargreaves Equation at Watershed Scale. Hydrol. Earth Syst. Sci. **2011**, 15, 2495–2508, doi:10.5194/hess-15-2495-2011.
59. Seo, Y.; Lim, S.; Heo, S.; Yoon, B.; Hong, S.; Park, Y.; Hong, D. Modification of Hargreaves Equation Coefficient to Estimate Reference Evapotranspiration in Gangwondo. Korean J. Soil. Sci. Fert. **2019**, 52, 1–10, doi:10.7745/KJSSF.2019.52.1.001.
60. Muhammad, H.; Alamgir, A.K. Assessment of Hargreaves and Blaney-Criddle Methods to Estimate Reference Evapotranspiration Under Coastal Conditions. American Journal of Science, Engineering and Technology **2019**, 3, 65–72, doi:10.11648/j.ajset.20180304.11.
61. Trajkovic, S.; Kolakovic, S. Estimating Reference Evapotranspiration Using Limited Weather Data. J. Irrig. Drain Eng. **2009**, 135, 443–449, doi:10.1061/(ASCE)IR.1943-4774.0000094.
62. Trajkovic, S.; Kolakovic, S. Evaluation of Reference Evapotranspiration Equations Under Humid Conditions. Water Resour Manage **2009**, 23, 3057–3067, doi:10.1007/s11269-009-9423-4.
63. Yang, Q.; Ma, Z.; Zheng, Z.; Duan, Y. Sensitivity of Potential Evapotranspiration Estimation to the Thornthwaite and Penman–Monteith Methods in the Study of Global Drylands. Adv. Atmos. Sci. **2017**, 34, 1381–1394, doi:10.1007/s00376-017-6313-1.
64. Castañeda, L.; Rao, P. Comparison of methods for estimating reference evapotranspiration in Southern California. J. Environ. Hydrol. **2005**, 13, 1–10, Corpus ID: 131246841.
65. Aschonitis, V.; Touloumidis, D.; ten Veldhuis, M.C.; Coenders-Gerrits, M. Correcting Thornthwaite potential evapotranspiration using a global grid of local coefficients to support temperature-based estimations of reference evapotranspiration and aridity indices. Earth Syst. Sci. Data **2022**, 14, 163–177, doi:10.5194/essd-14-163-2022.
66. Camargo, A.P.; Marin, F.; Sentelhas, P.C.; Picini, AG. Adjust of the Thornthwaite's method to estimate the potential evapotranspiration for arid and superhumid climates, based on daily temperature amplitude. Rev. Bras. Agrometeorol. **1999**, 7. 251-257.
67. Noguera, I.; Vicente-Serrano, S.M.; Domínguez-Castro, F. The Rise of Atmospheric Evaporative Demand Is Increasing Flash Droughts in Spain During the Warm Season. Geophysical Research Letters **2022**, 49, e2021GL097703, doi:10.1029/2021GL097703.
68. Massari, C.; Avanzi, F.; Bruno, G.; Gabellani, S.; Penna, D.; Camici, S. Evaporation Enhancement Drives the European Water-Budget Deficit during Multi-Year Droughts. Hydrol. Earth Syst. Sci. **2022**, 26, 1527–1543, doi:10.5194/hess-26-1527-2022.
69. Greve, P.; Kahil, T.; Mochizuki, J.; Schinko, T.; Satoh, Y.; Burek, P.; Fischer, G.; Tramberend, S.; Burtscher, R.; Langan, S.; et al. Global Assessment of Water Challenges under Uncertainty in Water Scarcity Projections. Nat Sustain **2018**, 1, 486–494, doi:10.1038/s41893-018-0134-9.

70. Konapala, G.; Mishra, A.K.; Wada, Y.; Mann, M.E. Climate Change Will Affect Global Water Availability through Compounding Changes in Seasonal Precipitation and Evaporation. Nat Commun **2020**, 11, 3044, doi:10.1038/s41467-020-16757-w.

Disclaimer/Publisher's Note: The statements, opinions and data contained in all publications are solely those of the individual author(s) and contributor(s) and not of MDPI and/or the editor(s). MDPI and/or the editor(s) disclaim responsibility for any injury to people or property resulting from any ideas, methods, instructions or products referred to in the content.